J. Fluid Mech. (1988), *vol.* 192, *pp.* 33–50
Printed in Great Britain

Models for very wide-angle water waves and wave diffraction

By ROBERT A. DALRYMPLE† AND JAMES T. KIRBY‡

†Ocean Engineering Group, Department of Civil Engineering, University of Delaware, Newark, DE 19716, USA

‡Coastal and Oceanographic Engineering Department, University of Florida, Gainesville, FL 32601, USA

(Received 23 March 1987 and in revised form 12 November 1987)

For a bathymetry consisting of parallel bottom contours, wide-angle parabolic models are developed to describe the diffraction of linear water waves. The first model, developed by operator correspondence, extends the validity of conventional forms of the parabolic model for wave angles up to 70° from the assumed wave direction. Through the use of Fourier decomposition, wave models valid to 90° are developed for three different lateral boundary conditions. By application, it is shown that the diffraction of waves through gaps or around structures is governed by the initial wave condition at the structure, which can be expanded into progressive and evanescent wave modes. Away from the structure, the wave field consists of only the progressive wave modes, which disperse according to their direction of propagation, the water depth and Snell's Law. Examples are shown for oblique waves through a gap, directional seas past a breakwater, a plane wave with varying crest amplitude, and finally for the diffraction of waves into a channel.

1. Introduction

The parabolic method for wave propagation has proven to be very effective in providing a convenient and rapid method for the calculation of the surface wave field over water of varying depths, including such important phenomena as refraction and diffraction, e.g. Radder (1979), Booij (1981), Kirby & Dalrymple (1983, 1984) and Liu & Tsay (1984). There is a significant drawback of the method, however, in that it requires that the waves propagate (nearly) in a given direction (taken here to be the x-direction). This restriction limits the application of the method, particularly when the transmission of the wave motion past an obstacle is desired, as often strong diffraction occurs in the rear of the obstacle. As an example, Kirby & Dalrymple (1986) shows an analytic solution to a simple parabolic model for waves behind an offshore breakwater. Their solution is similar to a Fresnel approximation for light passing through a slit, yielding far-field results that are reasonable, but the near-field results are in error.

There are several methods for the development of wide-angle approximation models. Here, Fourier transforms are used to treat the case of waves propagating in water depths characterized by parallel bottom contours.

This paper will first provide the background for parabolic models, valid for constant depth, illustrating the limitation at present on the propagation directions of the waves. A wide-angle model will be developed for this case. In §3, a new model for variable depth, based on eigenfunction decomposition is derived. Section 3 also

illustrates the results of the model in several idealized situations, such as waves through a breakwater gap, and §4 discusses the interpretation of wave diffraction, using the Fourier decomposition.

2. Background

For constant-depth water, Mei & Tuck (1980) developed a linear parabolic model for use with waves propagating past slender bodies. Their model is developed from the Laplace equation by expressing the velocity potential Φ as

$$\Phi(x, y, z, t) = A(x, y) f(z, h)\, e^{i(kx-\omega t)}, \tag{2.1}$$

where

$$f(z, h) = \frac{\cosh k(h+z)}{\cosh kh}. \tag{2.2}$$

The amplitude A varies spatially owing to the presence of the body, and k and ω are the wavenumber and angular frequency of the wave. The coordinate system is oriented with the x- and y-axes in the horizontal plane and z points upward from the still water surface. It is assumed that the waves will propagate primarily in the $+x$-direction.

The velocity potential Φ must satisfy the usual linear boundary-value problem for water waves which gives the Laplace equation for the potential. The wavenumber k must satisfy the dispersion relationship, which relates the wave angular frequency ω to the water depth h, and k:

$$\omega^2 = gk \tanh kh. \tag{2.3}$$

Substituting the assumed form of Φ into Laplace's equation, we obtain an equation for the amplitude:

$$A_{xx} + 2ikA_x + A_{yy} = 0. \tag{2.4}$$

Mei & Tuck showed by scaling x and y by the length of the slender body, L, that the A_{xx} term may be dropped provided that $kL \gg 1$. This leaves us with

$$2ikA_x + A_{yy} = 0. \tag{2.5}$$

This is the simple parabolic approximation to (2.4), which provides some obvious advantages, including the reduction in the number of boundary conditions necessary for a solution and a significant computational advantage in that this parabolic equation is easier to solve than the elliptic equation.

A graphic interpretation of the validity of the parabolic method is obtained (following Claerbout 1985) by assuming a plane-wave solution, propagating at an angle to the x-axis, say,

$$A = a\, e^{i\{(l-k)x+my\}}, \tag{2.6}$$

where $l = k\cos\theta$ and $m = k\sin\theta$, and θ is the angle between the wave propagation direction and the x-axis. Substituting (2.6) into the parabolic equation, we have

$$2k(l-k) + m^2 = 0. \tag{2.7}$$

The relationship between l and m is a parabola. On the other hand, from the Laplace equation (or (2.4)), we have the exact relationship between the wavenumber components:

$$l^2 + m^2 - k^2 = 0, \tag{2.8}$$

which describes a circle. The parabolic model only has the same geometric relationship when $m = 0$. These two relationships are shown in figure 1.

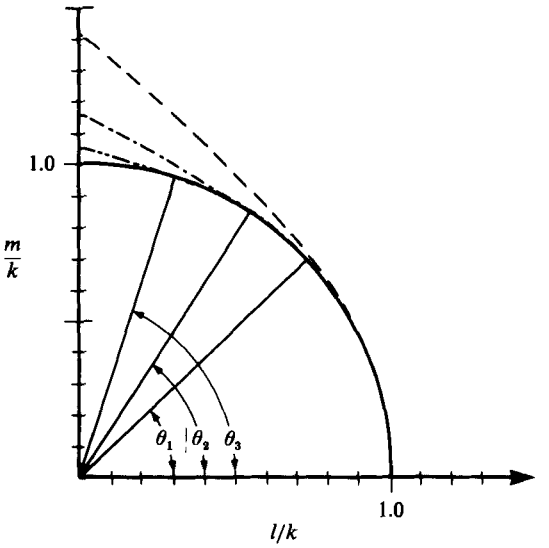

FIGURE 1. Comparison of parabolic-model wavenumber relationships to the (unit circle) exact solution. -----, simple parabolic model (2.5); –·–·–, Booij model (2.9); –·–·–·– (2.16).

One measure of the error in the parabolic equation is the deviation of the parabolic curve from the circle. For a given m, the parabolic method tends to overestimate l, except in the vicinity of $\theta = 0$, where θ is the wave propagation angle to the x-axis. This overestimation means that waves with a given m will not be turned towards the y-axis as much as they should. If an error in l is defined as $(l-l_e)/l_e \times 100\,\%$, where l_e is the exact value of l for a given m, then the errors can be quantified. The simple parabolic model can accurately predict the propagation of plane waves with angles up to 43°, without creating more than a 5% error in l. This angle is shown as θ_1 in figure 1.

Booij (1981) developed a wide-angle parabolic model, extending the original parabolic equation of Radder (1979) for variable water depth to wider wave angles. For constant water depth, this model is

$$2ikA_x + A_{yy} + iA_{xyy}/2k = 0. \tag{2.9}$$

Dingemans (1983) and Kirby (1986*a*) provide a justification for Booij's model in terms of a (1, 1) Padé approximant of the exact relationship (2.8). As shown in figure 1, Booij's correction permits wider propagation angles than the simple parabolic model. Using the error criterion given above, waves are adequately modelled for up to $\theta_2 = 56.5°$ from the x-axis, a 13.5° improvement. A numerical model of this equation (even including other terms to account for changes in water depth, for example) can be conveniently developed using a Crank–Nicolson technique (Booij 1981; Kirby & Dalrymple 1983, 1984).

Kirby (1986*b*) provides a (2, 2) Padé approximant, which, by use of operator correspondence, can be written as

$$2ikA_x + A_{yy} - \frac{3A_{xyy}}{2ik} - \frac{A_{xyyyy}}{8ik^3} + \frac{A_{yyyy}}{2k^2} = 0. \tag{2.10}$$

This equation is reasonably accurate out to large angles (70°). Table 1 shows predicted values of wavenumber in the y-direction (m/k) as a function of l/k.

l/k	$m/k = (1-(l/k)^2)^{\frac{1}{2}}$	m/k (2.10)	m/k (2.11)	m/k (2.16)
0	1.0	1.05146	1.11333	1.05977
0.2	0.979079	1.0000	1.03827	1.0000
0.5	0.86602	0.86852	0.87972	0.86288
0.8	0.6	0.6000362	0.60064	0.59818
0.9	0.43589	0.43589	0.43595	0.43545
1.0	0	0	0	0

TABLE 1. Comparison of the wide-angle equations to the exact relationship

McAninch (1986), studying the propagation of acoustic waves, used an integrating factor of e^{2ikx} to integrate (2.5) by parts. This yields equations with as many terms in A as desired, with an integral error term at the end. For example, we can examine

$$2ikA_x + A_{yy} + \frac{iA_{xyy}}{2k} - \frac{A_{yyxx}}{4k^2} + e^{-2ikx}\int \frac{e^{2ikx}A_{yyxxx}\,dx}{4k^2} = 0. \tag{2.11}$$

This equation can be shown to be exact for plane waves; however, the integral term, which is neglected, is as large as the last term and McAninch's equations do not resemble the expansions given above. Column 4 of table 1 shows the wavenumbers calculated by this approach. The method is not as accurate as those given previously.

Kirby (1986*b*) additionally utilized a minimax approach to find the best approximation for waves propagating at large angles from the x-direction. This approach gave up the exact solution for waves propagating directly in the x-direction in order to provide better accuracy for waves propagating at wider angles to the x-axis. His modified parabolic equation reads

$$2ikA_x + 2(b_1 - a_1)A_{yy} - \frac{2ib_1 A_{xyy}}{k} + 2k(a_0 - 1)A = 0 \tag{2.12}$$

where the values of a_0, a_1 and b_1 are found by requiring the error in l be minimized over a given range of wave angles. For example, for $0 < \theta < 60°$, Kirby found $a_0 = 0.998213736$, $a_1 = -0.854229482$, and $b_1 = -0.383183081$. (Note that the values from Booij's approximation yield $a_0 = 1$, $a_1 = -0.75$ and $b_1 = -0.25$.) The deviation of a_0 from unity indicates the error present for waves propagating in the x-direction. Here the wavenumber in the x-direction is multiplied by a_0, resulting in a wave that propagates faster than the exact solution; however, the discrepancy will make itself known only after long distances. The results of (2.12) at large angles are shown by Kirby (1986*b*) to be approximately as accurate as those of (2.10). This accuracy is obtained without extending the numerical complexity of the equations beyond the level commensurate with the (1, 1) Padé form (2.9).

2.1. *A heuristic development of a constant-depth wide-angle model*

A parabolic model, valid for large wave angles, should have a wavenumber relationship which approximates a circle. Following Claerbout, we solve the exact (2.8) for l and express it by a binomial expansion,

$$l = k - \frac{m^2}{2k} - \frac{m^4}{8k^3} - \frac{m^6}{16k^5} \cdots . \tag{2.13}$$

(The parabolic equation, solved for l, yields the first two terms of this series. A model to be valid for wide angles of propagation clearly needs to incorporate more terms in this binomial expansion.)

Using the method of operator correspondence, we can determine the governing equation for the wavenumber relation in (2.13). With $\phi_x = il\phi$ and $\phi_y = im\phi$, we can replace l and m by corresponding derivatives term by term. The governing equation is then

$$\phi_x = \mathrm{i}k\left(\phi + \frac{\phi_{yy}}{2k^2} - \frac{\phi_{yyyy}}{8k^4} + \frac{\phi_{yyyyyy}}{16k^6} \ldots\right). \tag{2.14}$$

Again replacing ϕ by the expression with A (2.1), we obtain

$$2\mathrm{i}kA_x + A_{yy} - \frac{A_{yyyy}}{4k^2} + \frac{A_{yyyyyy}}{8k^4} \ldots = 0. \tag{2.15}$$

This equation is a wide-angle parabolic approximation for constant depth (k fixed). We can develop another form of this equation by replacing A_{yy} with $-2\mathrm{i}kA_x$, which is the lowest-order approximation:

$$2\mathrm{i}kA_x + A_{yy} + \frac{\mathrm{i}A_{xyy}}{2k} - \frac{\mathrm{i}A_{xyyyy}}{4k^3} \ldots = 0. \tag{2.16}$$

Examining the errors generated by these last two approximations when compared to the exact solution, (2.16) with four terms and the x-derivatives is more accurate than (2.15), again with four terms. In fact, the last equation is nearly as good as the (2, 2) Padé approximant of Kirby, while (2.15) is somewhat better than the Booij approximation (the 5% error level occurs at 69°). The comparison of (2.16) with previous parabolic models is shown in figure 1 and in table 1. Despite the reasonable agreement, with $\theta_3 = 72°$, we can conclude that many terms must be included in a binomial expansion for high accuracy at large wave angles and that the substitution of $-2\mathrm{i}kA_x$ for A_{yy} provides greater accuracy in the wave modelling.

3. A solution for wide-angle diffraction over a variable topography

In this section, we shall derive a model valid for angles of propagation up to 90° and permit the depth to vary in the x-direction, in order to study the simultaneous diffraction and refraction of waves. The governing equation is the mild-slope equation developed by Berkhoff (1972), which has been used in the variable-depth parabolic models of Radder (1979), Kirby & Dalrymple (1983) and Liu & Tsai (1984). The equation governs the horizontal variation of the velocity potential Φ, written as $\Phi = \phi(x, y)f(z, h)\exp(-\mathrm{i}\omega t)$ (here ϕ plays a similar role as $A(x, y)$ in the previous section, but it absorbs the $\exp(\mathrm{i}kx)$ which was factored out before):

$$\nabla \cdot CC_g \nabla\phi + k^2 CC_g \phi = 0, \tag{3.1}$$

where

$$C = \omega/k, \quad C_g = \omega_k. \tag{3.2}$$

The dispersion relationship (2.3) is also needed to relate ω and k. The mild-slope equation is exact for deep, shallow and constant-depth water and Booij (1983) has shown that it is valid for intermediate depths as long as the depth does not change too rapidly over a wavelength. If the velocity product CC_g does not vary in the y-direction, then the Fourier transform of (3.1) in the y-direction leads to

$$(CC_g \hat{\phi}_x)_x + (k^2 - \lambda^2) CC_g \hat{\phi} = 0, \tag{3.3}$$

where the circumflex denotes a transformed variable and λ is the continuous Fourier parameter. This equation can be split by assuming

$$\hat{\phi}(x, \lambda) = \hat{\phi}^+ + \hat{\phi}^-, \tag{3.4}$$

where $\hat{\phi}^+$ is the transformed potential describing the forward-propagating waves and $\hat{\phi}^-$ describes the backscattered waves. Further we assume that we can split (3.3) into the following coupled first-order equations:

$$\hat{\phi}^+_x = \mathrm{i}(k^2-\lambda^2)^{\frac{1}{2}}\hat{\phi}^+ + F, \quad \hat{\phi}^-_x = -\mathrm{i}(k^2-\lambda^2)^{\frac{1}{2}}\hat{\phi}^- - F, \tag{3.5}$$

where $F(x, \lambda)$ is an unknown function. Substituting these expressions into (3.3) yields F:

$$F(x, \lambda) = \frac{-[CC_{\mathrm{g}}(k^2-\lambda^2)^{\frac{1}{2}}]_x}{2CC_{\mathrm{g}}(k^2-\lambda^2)^{\frac{1}{2}}}(\hat{\phi}^+ - \hat{\phi}^-). \tag{3.6}$$

It can be shown by back-substitution that (3.5) and (3.6) yield (3.3) identically and thus the splitting introduced here does not introduce the type of approximations associated with the pseudo-operators in the parabolic equation method. Neglecting the assumed small backscattered wave (ϕ^-), we obtain

$$\hat{\phi}^+_x = \mathrm{i}(k^2-\lambda^2)^{\frac{1}{2}}\hat{\phi}^+ - \frac{[CC_{\mathrm{g}}(k^2-\lambda^2)^{\frac{1}{2}}]_x\hat{\phi}^+}{2CC_{\mathrm{g}}(k^2-\lambda^2)^{\frac{1}{2}}}. \tag{3.7}$$

Expanding the last term and multiplying through by $2CC_{\mathrm{g}}$ puts the above equation into the more familiar parabolic form:

$$2CC_{\mathrm{g}}\hat{\phi}^+_x + (CC_{\mathrm{g}})_x\hat{\phi}^+ - 2\mathrm{i}CC_{\mathrm{g}}(k^2-\lambda^2)^{\frac{1}{2}}\hat{\phi}^+ + CC_{\mathrm{g}}\frac{[(k^2-\lambda^2)^{\frac{1}{2}}]_x\hat{\phi}^+}{(k^2-\lambda^2)^{\frac{1}{2}}} = 0. \tag{3.8}$$

This equation can be solved analytically, which, after the inverse Fourier transform, is expressed as

$$\Phi^+ = \frac{1}{2\pi}\int_{-\infty}^{\infty}\hat{A}(\lambda)\left[\frac{(CC_{\mathrm{g}})_0(k_0^2-\lambda_0^2)^{\frac{1}{2}}}{CC_{\mathrm{g}}(k^2-\lambda^2)^{\frac{1}{2}}}\right]^{\frac{1}{2}}\exp\left(\mathrm{i}\int(k^2-\lambda^2)^{\frac{1}{2}}\mathrm{d}x\right)\mathrm{e}^{\mathrm{i}\lambda y}\,\mathrm{d}\lambda\, f(z, h)\,\mathrm{e}^{-\mathrm{i}\omega t}, \tag{3.9}$$

where the depth-dependency term, f, is as defined in (2.2). The bracketed term contains the shoaling and refraction coefficients associated with gradual water depth changes (e.g. Dean & Dalrymple 1984), with the subscripts 0 indicating initial conditions at $x = 0$. In this solution, the $\hat{A}(\lambda)$ is the angular spectrum of the wave field (Booker & Clemmow 1950; Stamnes *et al.* 1983), which is the Fourier transform of the initial condition at $x = 0$, in terms of the Fourier parameter, λ.

For constant depth, the above equation simplifies to

$$\Phi^+(x, y, z, t) = \frac{1}{2\pi}\int_{-\infty}^{\infty}\hat{A}(\lambda)\,\mathrm{e}^{\mathrm{i}(k^2-\lambda^2)^{\frac{1}{2}}x}\,\mathrm{e}^{\mathrm{i}\lambda y}\,\mathrm{d}\lambda f(z, h)\,\mathrm{e}^{-\mathrm{i}\omega t}. \tag{3.10}$$

This equation shows that the wave potential at any location is composed of an infinite number of wavelets, each with amplitude, $\hat{A}(\lambda)\,\mathrm{d}\lambda/(2\pi)$ and travelling in the direction θ given by

$$\tan\theta = \lambda/(k^2-\lambda^2)^{\frac{1}{2}}$$

Introducing θ into (3.10) yields

$$\Phi^+(x, y, z, t) = \frac{1}{2\pi}\int_{-\frac{1}{2}\pi}^{\frac{1}{2}\pi}k\hat{A}(k\sin\theta)\,\mathrm{e}^{\mathrm{i}(k\cos\theta x + k\sin\theta y)}\,\mathrm{d}\theta f(z, h)\,\mathrm{e}^{-\mathrm{i}\omega t},$$

which is a form analogous to a directional wave spectrum. The analogy holds only for cases where the initial condition at $x = 0$ is defined over a small interval (Booker & Clemmow 1950) and where all the evanescent modes for which the magnitude of λ exceeds k are neglected.

We can compare (3.10) to the solution obtained from the simple parabolic approximation (2.5) which is (Kirby & Dalrymple 1986)

$$\Phi^+(x, y, z, t) = \frac{1}{2\pi}\int_{-\infty}^{\infty} \hat{A}(\lambda) \exp\left\{ik\left(1-\frac{\lambda^2}{2k^2}\right)x\right\} e^{i\lambda y}\, d\lambda f(z, h)\, e^{-i\omega t},$$

which results from approximating the square-root term in (3.10), leading to the small-angle restrictions discussed in §2. We note that the solutions of the parabolic models do not have evanescent modes; waves with $\lambda > k$ also propagate freely in the solution domain (Kirby 1986*b*).

In water of variable depth, for the simple case of a single wave train, the multiple-scales solution of Mei, Tlapa & Eagleson (1968) is obtained readily for the initial conditions:

$$\left.\begin{aligned} A(0, y) &= A_0\, e^{i\lambda_0 y} \\ \text{and} \qquad \hat{A}(\lambda) &= 2\pi\delta(\lambda-\lambda_0) A_0, \end{aligned}\right\} \tag{3.11}$$

with $\lambda_0 = k \sin\theta_0$, the projection of the wavenumber on the y-axis. However, for more difficult problems, involving complicated initial conditions, the solution is more easily solved quasi-numerically. Here we use discrete Fourier transforms, which impose periodic lateral boundary conditions in the y-direction. The initial conditions $\hat{A}(\lambda)$ are obtained along the initial row ($x = 0$), consisting of N columns, by using a fast Fourier transform (FFT) on the digitized values of $A(0, (m-1)\Delta y)$, where $m = 1$ to N. Then for each x and y location, $\hat{\phi}^+$ is computed using the integrand of (3.9), with the argument of the exponential computed using a simple Euler integration in x. To determine the final wave potential on a row, the inverse FFT is used.

The evolution of the wave field is in part governed by the decay of evanescent terms in (3.9). The FFT of the initial condition yields wave components with values of λ ranging from zero to a maximum of $\pi/\Delta y$ (the Nyquist wavenumber for the given digitization in the y-direction). Many of these wavenumbers do not correspond to progressive waves as they exceed k in magnitude. These waves decay exponentially in the propagation direction. Only those waves for which $|\lambda| \leqslant k$ persist far into the domain. (Therefore care must be taken to choose the Δy and the number of terms in the FFT. For example, for plane waves over constant depth, very few terms are needed if the desired wave corresponds to one of the λ in the FFT, $\lambda_m = \{2\pi m/(N\Delta y)$, $m = 1, 2, 3, \ldots\}$. If not, then N must be large enough so that the evanescent modes have negligible amplitude.)

With the FFT approach, the wave field far from the y-axis is composed simply of a finite number of plane waves travelling in different directions, each with an amplitude and phase given by the initial condition at $x = 0$.

3.1. *Constant-depth solutions*

In order to verify the model, it is compared to existing solutions for constant depth. Three cases are studied: plane waves, the finite-length wavemaker problem and waves around an island.

With the initial conditions (3.11), which is the projection of a plane wave on the y-axis, the solution is

$$\Phi(x, y, z, t) = A_0 \, \mathrm{e}^{\mathrm{i}(k^2-\lambda_0^2)^{\frac{1}{2}}x} f(z, h) \, \mathrm{e}^{\mathrm{i}(\lambda_0 y-\omega t)}, \tag{3.12}$$

where f is as defined in (2.2). This equation is the *exact* solution for plane waves travelling at an angle, $\theta = \sin^{-1}(\lambda_0/k)$, to the x-axis; there is no difficulty with large angles, and the propagation angle may extend to 90°. Column 1 of table 1 for the exact solution is valid for this solution as well. The relevant governing equation for constant depth is (3.8) without the second and fourth terms, which result from depth variations.

In Dalrymple & Greenberg (1985), the problem of a finite-length wavemaker is given for the exact linear three-dimensional boundary-value problem. For the initial conditions,

$$\phi_x = \begin{cases} 0, & |y| > L, \\ \mathrm{e}^{\mathrm{i}\lambda_0 y}, & |y| < L, \end{cases} \tag{3.13}$$

where it is assumed that the amplitude of the velocity associated with the progressive wave is unity. (No information is obtainable about the vertical evanescent modes in the present model, since we restricted the vertical dependency by the $f(z, h)$ factor. Stamnes (1986, §19.1) presents these modes.)

From (3.9), (3.12), we obtain

$$\Phi_x(0, y, z, t) = \frac{1}{2\pi} \int_{-\infty}^{\infty} \hat{A}(\lambda) \, \mathrm{i}(k^2-\lambda^2)^{\frac{1}{2}} \, \mathrm{e}^{\mathrm{i}\lambda y} \, \mathrm{d}\lambda f(z, h) \, \mathrm{e}^{-\mathrm{i}\omega t}. \tag{3.14}$$

Therefore,
$$\hat{\phi}_x(0, \lambda) = \mathrm{i}(k^2-\lambda^2)^{\frac{1}{2}} \hat{A}(\lambda)$$

and
$$\hat{A}(\lambda) = \frac{-2\mathrm{i} \sin(\lambda_0-\lambda) L}{(\lambda_0-\lambda)(k^2-\lambda^2)^{\frac{1}{2}}}. \tag{3.15}$$

Substituting into the equation for Φ, we have

$$\Phi(x, y, z, t) = \frac{-\mathrm{i}}{2\pi} \int_{-\infty}^{\infty} \frac{2 \sin(\lambda_0-\lambda) L}{(\lambda_0-\lambda)} \frac{\mathrm{e}^{\mathrm{i}(k^2-\lambda^2)^{\frac{1}{2}}x}}{(k^2-\lambda^2)^{\frac{1}{2}}} \mathrm{e}^{\mathrm{i}\lambda y} \, \mathrm{d}\lambda f(z, h) \, \mathrm{e}^{-\mathrm{i}\omega t} \tag{3.16}$$

or, by the convolution theorem,

$$\Phi(x, y, z, t) = \tfrac{1}{2}\mathrm{i} \int_{-L}^{L} \mathrm{e}^{\mathrm{i}\lambda\zeta} H_0^{(1)}(k[x^2+(y-\zeta)^2]^{\frac{1}{2}}) \, \mathrm{d}\zeta f \, \mathrm{e}^{-\mathrm{i}\omega t}. \tag{3.17}$$

This solution is identical to the result in Dalrymple & Greenberg for the progressive wave mode, which was obtained for the full three-dimensional problem. A Green-function solution to the same problem is presented in Appendix A.

The initial condition for waves behind a straight breakwater of length $2L$ is given by

$$\phi_x(0, y, z, t) = \begin{cases} \mathrm{e}^{\mathrm{i}\lambda_0 y}, & |y| > L, \\ 0, & |y| < L. \end{cases} \tag{3.18}$$

This problem is complementary to the wavemaker problem above; its solution, from Babinet's Principle in optics, is the plane-wave solution with the wavemaker solution subtracted from it. The result is a Rayleigh–Sommerfeld approximation to light passing through a gap, in that the reflection on the upwave side of the structure is neglected. This solution is more physically correct than that provided by Kirby &

Dalrymple (1986), as the wide-angle model is used and, further, the correct velocity boundary condition is used, rather than a zero potential condition along the breakwater.

3.2. *Diffraction in domains that are periodic in the lateral direction*

For laterally periodic domains, the problem is simplified somewhat, as the diffracted wave spectrum becomes discrete rather than continuous in λ. The complex finite Fourier-transform pair becomes

$$\hat{\phi}(x, n) = \frac{1}{2a}\int_{-a}^{a} \phi(x, y)\, \mathrm{e}^{-\mathrm{i}n\lambda y}\, \mathrm{d}y \tag{3.19a}$$

and

$$\Phi(x, y, z, t) = \sum_{n=-\infty}^{\infty} \hat{\phi}(x, n)\, \mathrm{e}^{\mathrm{i}n\lambda y} f(z, h)\, \mathrm{e}^{-\mathrm{i}\omega t}, \tag{3.19b}$$

where
$$\Phi(x, y, z, t) = \Phi(x, y+2a, z, t) \tag{3.20}$$

and
$$\lambda = \pi/a. \tag{3.21}$$

Following the same procedure as above, allowing for variable depth in the x-direction only, yields

$$\Phi^{+}(x, y, z, t) = \sum_{n=-N}^{N} A_n \left(\frac{(CC_{\mathrm{g}})_0 (k_0^2-(n\lambda)^2)^{\frac{1}{2}}}{CC_{\mathrm{g}}(k^2-(n\lambda)^2)^{\frac{1}{2}}}\right)^{\frac{1}{2}} \exp\left(\mathrm{i}\int^{x} [k^2-(n\lambda)^2]^{\frac{1}{2}}\,\mathrm{d}x\right) \mathrm{e}^{\mathrm{i}n\lambda y} f\, \mathrm{e}^{-\mathrm{i}\omega t}. \tag{3.22}$$

In this case, again, there is only a finite number of progressive waves that describe the wave field away from the y-axis.

3.2.1. *Periodic gaps in breakwaters*

The wavemaker problem, as specified in (3.13) is analogous to waves through a gap in a breakwater, when the Kirchhoff approximation is made. Carrying out the matching at $x = 0$ yields

$$A_n = \frac{-\mathrm{i}\sin(\lambda_0 - n\lambda)L}{(k^2-(n\lambda)^2)^{\frac{1}{2}}(\lambda_0 - n\lambda)a}, \tag{3.23}$$

where L is the half-width of the gap. For speed in computation, the fast Fourier transform is used. The initial conditions on the wave potential are approximated by an FFT of a top-hat function (of length corresponding to the gap width); then each wavenumber was multiplied by denominator in (3.15). The final velocity was then normalized to unity.

The resultant wave field was calculated for four different sloping bottoms, which are taken to be varying linearly in the x-direction. The wavemaker, lying along the y-axis in 10 m depth, has a length of 100 m. The incident wave field has a 9 s wave period and a 45° angle of incidence. The value of A along the wavemaker is taken as unity and $N = 128$, $\Delta x = \Delta y = 5$ m. In figure 2, the variation with bottom slope of the transmission coefficient (defined as the ratio of the local wave amplitude to the incident wave amplitude), corresponding to the value of 0.6, is shown. As the bottom slope increases from zero, the 0.6 contour elongates in the x-direction and bends towards the x-axis, as a result of wave refraction and shoaling on the slope. For the steepest slope the contour is not closed; it opens to encompass the entire y-axis as shoaling has become more influential than diffraction in the shallow water.

A measure of the bottom slope is the ratio, $\nabla h/k_0 h_0$, where the subscripts denote

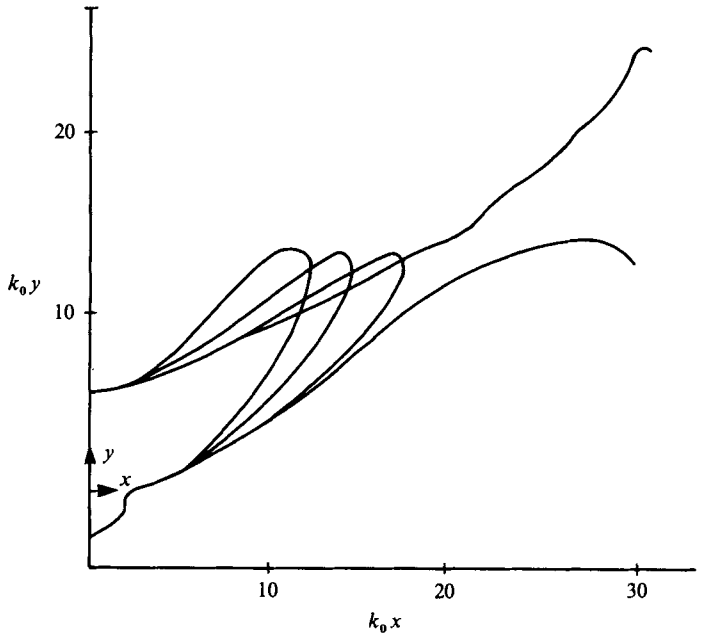

FIGURE 2. Effects of refraction and shoaling on the transmission coefficient (0.6) for periodic breakwater gaps. k_0 is the wavenumber at the breakwater, $k_0 = 0.07688$ m^{-1}.

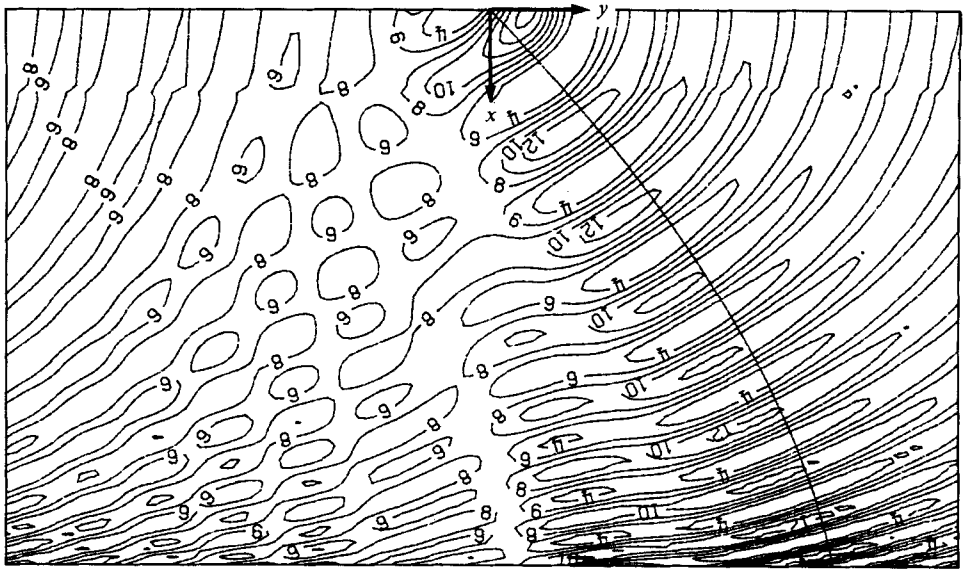

FIGURE 3. Instantaneous wave field behind periodic breakwater gaps on a sloping beach. The line denotes a wave ray, emanating from the centre of one of the gaps. Depicted area is 692.48 m (y-direction) × 405.75 m (x-direction).

values at $x = 0$. The mild-slope equation was derived with the assumption that the ratio is much less than unity. The four values for the figure are 0, 0.0162, 0.0260 and 0.0308.

In figure 3, the wave field associated with the steepest bottom slope is shown. The influence of wave refraction is clear, with the maximum of the diffraction pattern

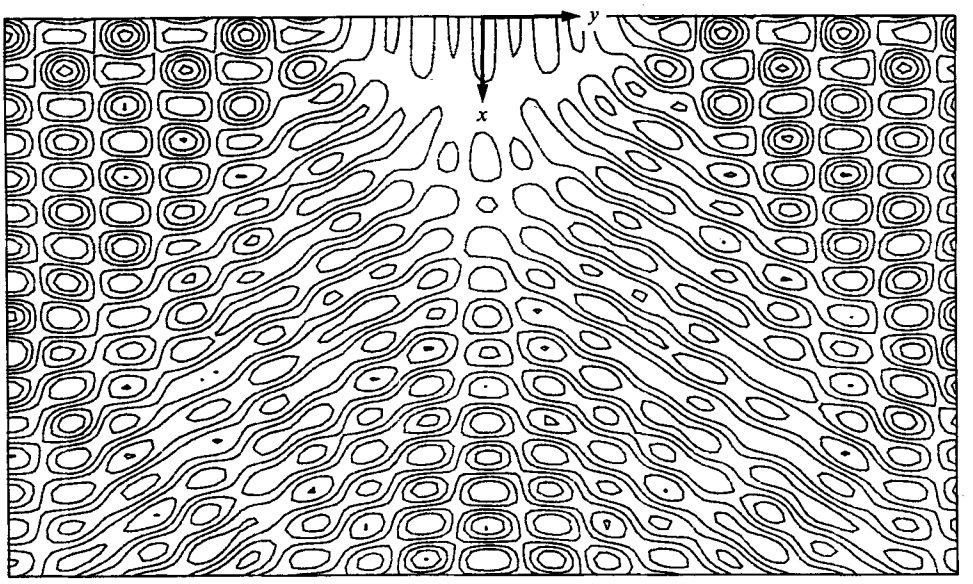

FIGURE 4. Instantaneous wave field behind an offshore breakwater created by two intersecting wave trains. The breakwater length is 386 m (in the y-direction) and the displayed area is 1016 m wide.

turning towards the shoreline normal. The influence of the periodic boundary conditions is also apparent as the waves from the down-wave gap have intruded into the figure. The wave ray $y(x)$, shown in the figure, was determined independently using the method outlined in Mei (1983),

$$\frac{\mathrm{d}y}{\mathrm{d}x} = \frac{\lambda_0}{(k^2 - \lambda_0^2)^{\frac{1}{2}}}, \tag{3.24}$$

which was solved by a Runge–Kutta integration. The diffracting wavetrain follows the wave ray very well.

3.2.2. *Intersecting waves past a breakwater*

The specification of the incident wave field can be quite general. As a simple example, two synchronous wavetrains are assumed to be incident on a breakwater (386.5 m in length, lying on the y-axis) by replacing the exponential term in the initial condition (3.18) with a cosine. In figure 4, the waves (period is 9 s) propagate at 30° to each side of the x-axis, creating a short-crested sea state in the absence of the breakwater. Behind the breakwater, centred in the middle of the y-axis, the two shadow zones cast by the two wavetrains result in a long-crested sea state in these zones, as only one of the wavetrains is blocked by the breakwater.

Extension to a truly directional sea state behind a breakwater composed of many frequencies is straightforward. It is a matter of superimposing the requisite number of wavetrains, with the appropriate random phases.

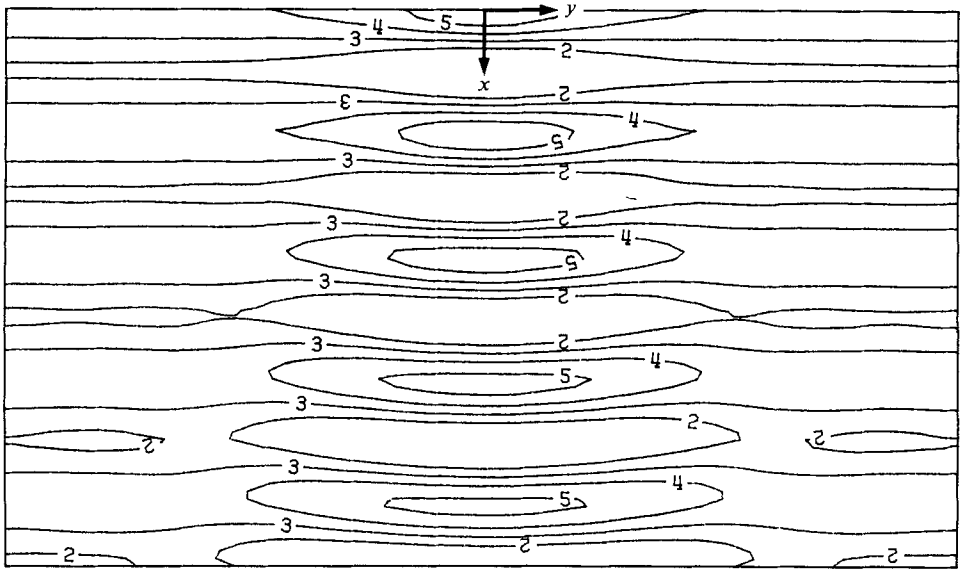

FIGURE 5. Instantaneous wave field for the example of plane-wave amplitude variation. Displayed area is 640 m × 375 m.

3.2.3. *A variation in crest elevation*

The effect of diffraction on a crestwise variation of wave amplitude is examined by superimposing a hyperbolic variation onto a normally incident wave, propagating over constant depth. The initial wave amplitude is described by

$$A(0, y) = 1 + 2\,\mathrm{sech}^2(\alpha y), \tag{3.25}$$

where α is 0.2. Again, the wave period is 9 s and the water depth is 10 m. The resulting water-surface elevation and the transmission coefficient are shown in figures 5 and 6. The effect of curvature in the wave amplitude at the outset causes the waves to change direction. This can be examined by examining the eikonal equation for the mild-slope equation, obtained by substituting

$$\phi = A\,\mathrm{e}^{\mathrm{i}S} \tag{3.26a}$$

into (3.1), where $A(x, y)$ and $S(x, y)$ are both real:

$$|\nabla S|^2 = k^2 + \frac{\nabla\cdot(CC_g\nabla A)}{CC_g A}. \tag{3.26b}$$

For constant depth, k is constant and the curvature of the wave crest in the y-direction results in the wave propagating slightly faster at the peak of the crest perturbation. On the side slopes of the perturbation, the crest curvature is of the opposite sign and the wave slightly slows there, resulting in a wave form that develops into a 'w'-shape as it propagates away from the origin. This is evident in figure 5. The result of this change in direction is a spreading of the wave height and wave energy away from the x-axis.

The influence of the amplitude on the wave direction and celerity was first noticed by Biesel (1964) and codified in this form by Battjes (1968). Both authors examined the effect as applied to Sommerfeld's semi-infinite-barrier problem (see Penney & Price 1952).

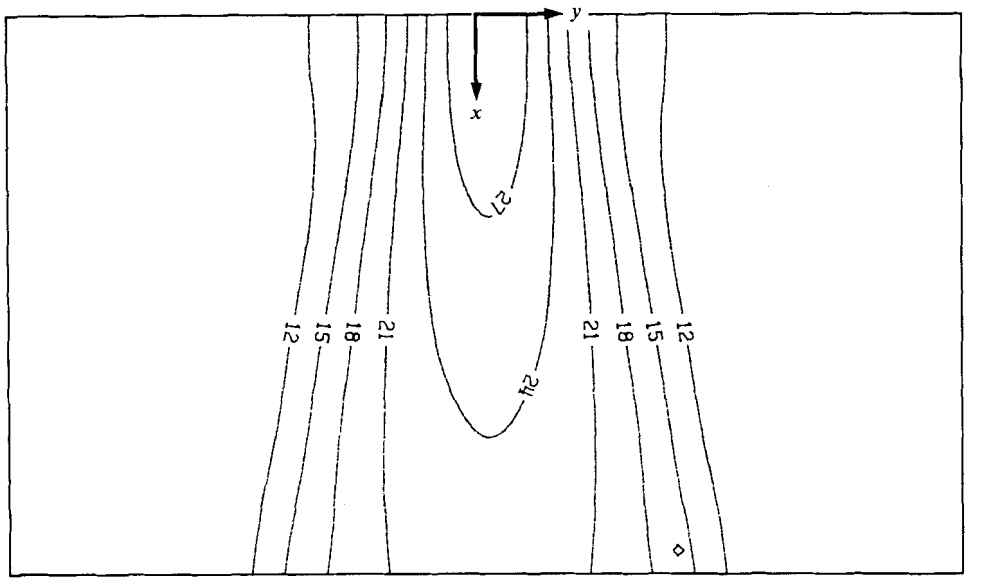

FIGURE 6. Transmission coefficient for the example of plane-wave amplitude variation. Contour levels have been multiplied by 10.

3.3. *Diffraction in a channel*

Diffraction into a channel with impermeable sidewalls (at $y = \pm a$) becomes simpler mathematically as separation of variables may be used to solve the problem, which now has the lateral boundary conditions

$$\Phi_y(x, \pm a, z, t) = 0. \tag{3.27}$$

The solution is easily obtained by separating the solution into orthogonal odd and even parts, each of which is a Sturm–Liouville problem in the y-direction. The solution is easily shown to be

$$\Phi(x, y, z, t) = \Phi^{\mathrm{e}} + \Phi^{\mathrm{o}}, \tag{3.28}$$

where

$$\Phi^{\mathrm{e}} = \sum_{n=0}^{\infty} A_n \left(\frac{(CC_{\mathrm{g}})_0 (k_0^2 - \lambda_n^2)^{\frac{1}{2}}}{CC_{\mathrm{g}} (k^2 - \lambda_n^2)^{\frac{1}{2}}} \right)^{\frac{1}{2}} \exp\left[\mathrm{i} \int (k^2 - \lambda_n^2)^{\frac{1}{2}} \, \mathrm{d}x \right] \cos \lambda_n y f(z, h) \, \mathrm{e}^{-\mathrm{i}\omega t} \tag{3.29a}$$

$$\Phi^{\mathrm{o}} = \sum_{n=1}^{\infty} B_n \left(\frac{(CC_{\mathrm{g}})_0 (k_0^2 - \gamma_n^2)^{\frac{1}{2}}}{CC_{\mathrm{g}} (k^2 - \gamma_n^2)^{\frac{1}{2}}} \right)^{\frac{1}{2}} \exp\left[\mathrm{i} \int (k^2 - \gamma_n^2)^{\frac{1}{2}} \, \mathrm{d}x \right] \sin \gamma_n y f(z, h) \, \mathrm{e}^{-\mathrm{i}\omega t} \tag{3.29b}$$

and

$$\lambda_n = \frac{n\pi}{a}, \quad n = 0, 1, 2, \ldots; \quad \gamma_n = \frac{(n - \frac{1}{2})\pi}{a}, \quad n = 1, 2, 3, \ldots. \tag{3.30a, b}$$

These solutions are a generalization (to a sloping bottom and progressive waves) of the work of Madsen (1974), who studied three-dimensional standing waves generated by a wavemaker in a constant-depth wave tank.

For the breakwater-gap boundary conditions, the coefficients A_n and B_n are

$$A_n = \frac{-2\mathrm{i}(\lambda_0 \sin \lambda_0 L \cos \lambda_n L - \lambda_n \cos \lambda_0 L \sin \lambda_n L)}{(k^2 - \lambda_n^2)^{\frac{1}{2}} a (\lambda_0^2 - \lambda_n^2)}, \tag{3.31a}$$

$$B_n = \frac{2(\gamma_n \sin \lambda_0 L \cos \gamma_n L - \lambda_0 \cos \lambda_0 L \sin \gamma_n L)}{(k^2 - \gamma_n^2)^{\frac{1}{2}} a (\lambda_0^2 - \gamma_n^2)}. \tag{3.31b}$$

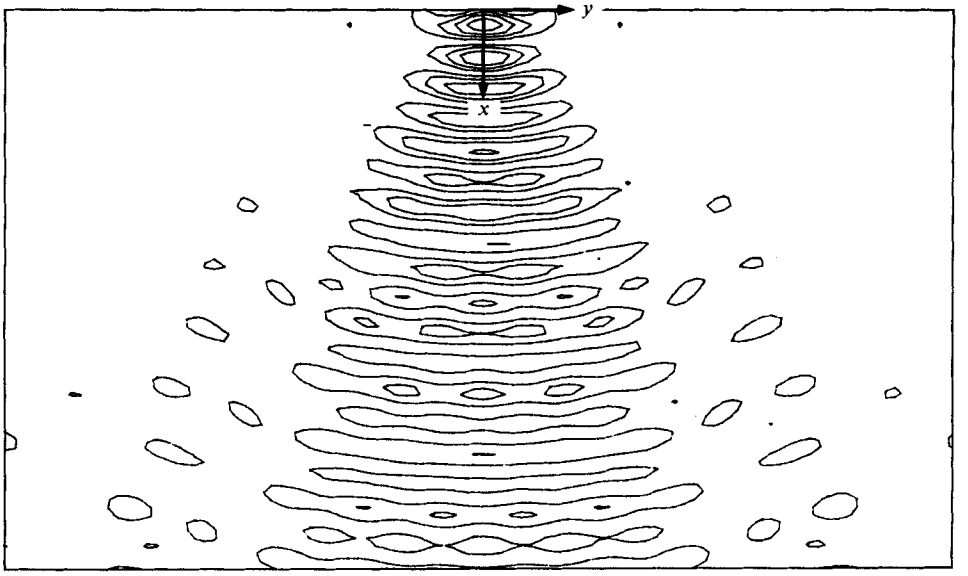

FIGURE 7. Propagation of a wavetrain through a gap into a channel for normal incidence. Displayed area is 1016 m wide, 762 m long. Contours are every 4 m.

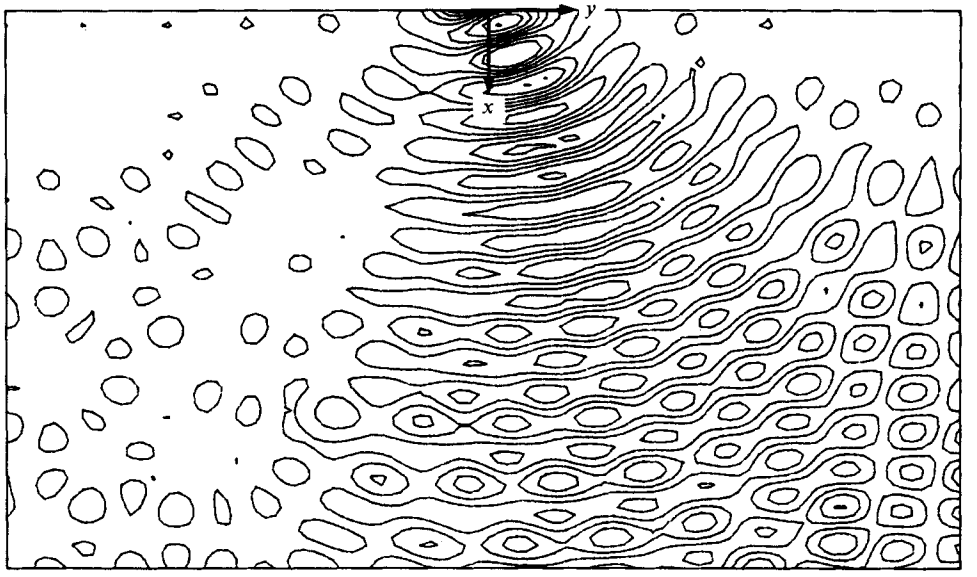

FIGURE 8. Propagation of a wavetrain through a gap into a channel for a 20° angle of incidence. Displayed area is 1016 m wide, 762 m long.

Two examples of this solution are shown in figures 7 and 8. The first is for normal incidence into a channel, 1016 m wide and a constant 10 m deep, and a gap of width 100 m. The influence of the channel sidewalls becomes important far from the gap. For this case, only 20 terms for each series are needed as the remainder of the terms in the infinite series are evanescent. Figure 8 is for 20° angle of incidence at the gap. As the diffracted waves impinge on the sidewall, reflection occurs, which results in a short-crested wave pattern. Since the model is valid up to 90° angles, the reflection pattern is set up very rapidly in the model, as shown in figure 8.

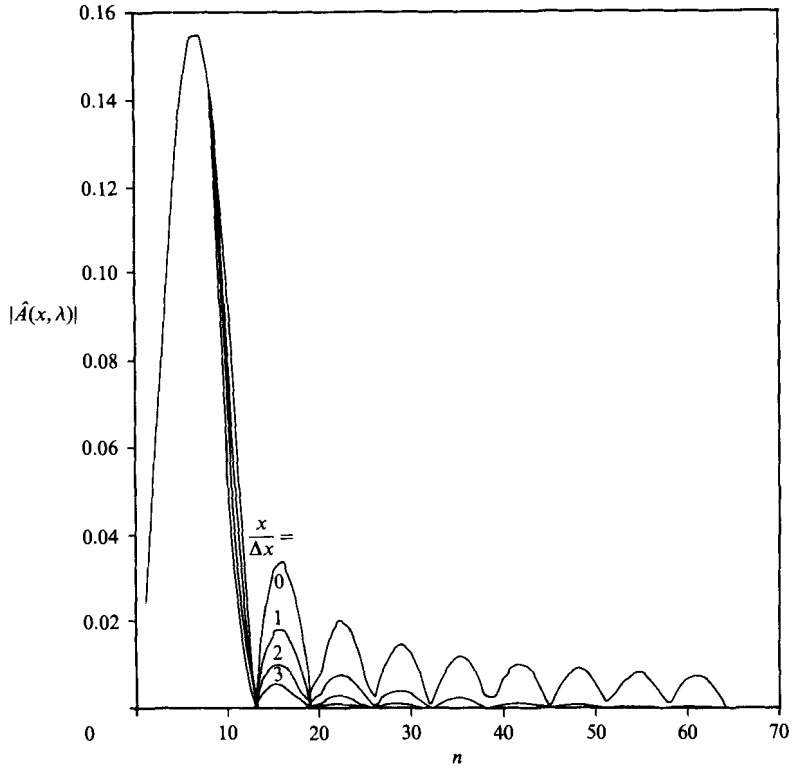

FIGURE 9. An example of the amplitude spectral modification with distance from breakwater gap (Figure 3). Curves decrease monotonically with each Δx. ($\Delta x = 5.41$ m.)

4. Conclusion and discussion

Wide-angle models permit the prediction of wave characteristics in regions where diffraction is very strong, such as might occur in front of wavemakers and behind breakwaters or offshore islands. For depths varying in the x-direction only, the initial wave field at $x = 0$ is resolved into Fourier components, which then propagate independently in the x-direction with wave phase functions dependent on k and λ alone, and not gradients of wave amplitude, as might be expected from (3.26*b*), which governs the total wave field. The Fourier components are not affected by the curvature of the wave crest; the associated eikonal equation for these wave components is simply

$$S_x = (k^2 - \lambda^2)^{\frac{1}{2}}, \tag{4.1}$$

found from the integrand of (3.9). Snell's law is exactly satisfied by these progressive modes; the wavenumber λ remains constant during the shoaling process.

Those waves with wavenumbers in the y-direction exceeding the wavenumber k are evanescent and most of these decay rather rapidly (within several Δx, where we have taken $\Delta x = \Delta y$). Thus, the evolving wave field in a diffracting domain is a result of the decay of the evanescent modes and the angular dispersion of the progressive modes, as they all propagate in different directions.

As an example of the decay of the Fourier components, the amplitude spectra, $|\hat{A}(x, \lambda)|$ (defined as the integrand of (3.9), excluding the exponential terms) of the waves in figures 2 and 3 are shown for $m = 1$ to $\frac{1}{2}N$ in figure 9. The uppermost curve shows the initial amplitude spectrum at $x = 0$, while the remaining curves are for

$x = n\Delta x$, $n = 1, 2, 3$. The rapid decay of the evanescent modes is obvious, occurring over distances much shorter than a wavelength (approximately $15\Delta x$ for this case).

The derivations and results here are for linear theory. The influence of wave amplitude on wave celerity and direction are well known and can affect very strongly the results shown here. These models will remain valid as long as the ratio of diffraction terms to the nonlinearity is large, or

$$\frac{\nabla\cdot(CC_g\nabla A)}{CC_g} \gg K|A|^2, \tag{4.2}$$

where
$$K = k^3\frac{C}{C_g}\left[\frac{\cosh 4kh + 8 - 2\tanh^2 kh}{8\sinh^4 kh}\right].$$

This relationship is obtained from the eikonal equation for the nonlinear mild-slope equation developed by Kirby & Dalrymple (1984).

Partial support for this research was provided to RAD by the NOAA Office of Sea Grant, Department of Commerce under Grant NA86AA-D-SG040. JTK acknowledges the support of the Office of Naval Research through Grant N00014-86-K-0790.

Appendix A. A Green-function approach to the constant-depth wave potential

Using Green's Second Identity, we can readily derive Weber's two-dimensional analogue to the Helmholtz Theorem (Baker & Copson 1950),

$$\phi(x, y) = -\tfrac{1}{4}\mathrm{i}\int_S\left(\phi\frac{\partial G}{\partial n} - G\frac{\partial\phi}{\partial n}\right)\mathrm{d}s, \tag{A 1}$$

where $G(x, y; \eta, \zeta) = H_0^{(1)}(kr_1)$, the Hankel function of the first kind; $r_1 = [(\eta-x)^2 + (\zeta-y)^2]^{\frac{1}{2}}$, the distance from the boundary point (η, ζ), to (x, y), and the normal derivatives are positive outward from the domain boundary, S. The line integral in this case encompasses the half-plane, $x > 0$. This equation has been used in the study of harbour resonance by Lee (1971). For $\phi(x, y)$, which satisfies the Sommerfeld radiation condition, the integral (A 1) is reduced to an integral along the y-axis ($x = 0$):

$$\phi(x, y) = \tfrac{1}{4}\mathrm{i}\int_{-\infty}^{\infty}\left(\phi(x, y, 0, \zeta)\frac{\partial G}{\partial x} - G(x, y, 0, \zeta)\frac{\partial\phi}{\partial x}\right)\mathrm{d}\zeta. \tag{A 2}$$

Alternative solutions that do not require ϕ or its derivative along the axis are obtained with a Green function that is zero (or its normal derivative is zero) along the y-axis.

The two possibilities are

$$G^- = H_0^{(1)}(kr_1) - H_0^{(1)}(kr_2), \tag{A 3}$$

where $r_2 = [(\eta+x)^2 + (\zeta-y)^2]^{\frac{1}{2}}$, the distance from the boundary point to an image point about the y-axis, or

$$G^+ = H_0^{(1)}(kr_1) + H_0^{(1)}(kr_2). \tag{A 4}$$

Substituting these into (A 2),

$$\phi(x, y) = -\tfrac{1}{2}\mathrm{i}\int_{-\infty}^{\infty} \phi(0, \eta) H_1^{(1)}[k(x^2+(y-\zeta)^2)]^{\frac{1}{2}} \frac{kx}{[x^2+(y-\zeta)^2]^{\frac{1}{2}}}\,\mathrm{d}\zeta \tag{A 5}$$

and

$$\phi(x, y) = \tfrac{1}{2}\mathrm{i}\int_{-\infty}^{\infty} \frac{\partial\phi}{\partial x}(0, \eta) H_0^{(1)}[k(x^2+(y-\zeta)^2)^{\frac{1}{2}}]\,\mathrm{d}\zeta. \tag{A 6}$$

The last equation is the same as (3.17).

REFERENCES

BAKER, B. B. & COPSON, E. T. 1950 *The Mathematical Theory of Huygen's Principle*, 2nd edn. Oxford University Press, 192 pp.

BATTJES, J. A. 1968 Refraction of water waves. *J. Waterways Harbors Div., ASCE*, **94** (WW4), 437–451.

BERKHOFF, J. C. W. 1972 Computation of combined refraction–diffraction. *Proc. 13th Intl Conf. Coastal Engng, ASCE, Vancouver*, pp. 471–490.

BIESEL, F. 1964 Equations approchées de la réfraction de la houle. In *Proc. 9th Intl Conf. Coastal Engng, ASCE, Lisbon*, pp. 55–69.

BOOIJ, N. 1981 Gravity waves on water with non-uniform depth and current. *Rep. 81–1.* Dept of Civil Eng., Delft University of Technology.

BOOIJ, N. 1983 A note on the accuracy of the mild-slope equation. *Coastal Engng* **7**, 191–203.

BOOKER, H. G. & CLEMMOW, P. C. 1950 The concept of an angular spectrum of plane waves, and its relation to that of polar diagram and aperture distribution. *Proc. Inst. Elect. Engrs.* Part III, **97**, 11–17.

CLAERBOUT, F. 1985 *Fundamentals of Geophysical Data Processing, with Application to Petroleum Prospecting.* Palo Alto: Blackwell Scientific, 274 pp.

DALRYMPLE, R. A. & GREENBERG, M. 1985 Directional wavemakers. In *Physical Modelling in Coastal Engineering* (ed. R. A. Dalrymple). A. A. Balkema.

DEAN, R. G. & DALRYMPLE, R. A. 1984 *Water Wave Mechanics for Engineers and Scientists.* Englewood Cliffs: Prentice-Hall, 353 pp.

DINGEMANS, M. W. 1983 Verification of numerical wave propagation models with field measurements: CREDIZ verification Haringvliet. *Rep. W488*, pt. 1. Delft Hydraul. Lab., Delft.

KIRBY, J. T. 1986*a* Higher-order approximations in the parabolic equation method for water waves. *J. Geophys. Res.* **91**, 933–952.

KIRBY, J. T. 1986*b* Rational approximations in the parabolic equation method for water waves. *Coastal Engng*, **10**, 355–378.

KIRBY, J. T. & DALRYMPLE, R. A. 1983 A parabolic equation for the combined refraction–diffraction of Stokes waves by mildly varying topography. *J. Fluid Mech.* **136**, 453–466.

KIRBY, J. T. & DALRYMPLE, R. A. 1984 Verification of a parabolic equation for propagation of weakly-nonlinear waves. *Coastal Engng*, **8**, 219–232.

KIRBY, J. T. & DALRYMPLE, R. A. 1986 Modeling waves in surfzones and around islands. *J. Waterway, Port, Coastal Ocean Engng, ASCE*, **112**, 78–93.

LEE, J.-J. 1971 Wave induced oscillations in harbours of arbitrary geometry. *J. Fluid Mech.* **45**, 375–394.

LIU, P. L.-F. & TSAY, T. K. 1984 Refraction–diffraction model for weakly nonlinear water waves. *J. Fluid Mech.* **141**, 265–274.

MADSEN, O. S. 1974 A three dimensional wavemaker, its theory and application. *J. Hydraulic Res.*, **12**, 205–222.

MCANINCH, G. L. 1986 Higher order parabolic approximations for sound propagation in stratified moving media. *AIAA J.* **24**, 2.

MEI, C. C. 1983 *The Applied Dynamics of Ocean Surface Waves.* Wiley-Interscience, 740 pp.

MEI, C. C., TLAPA, G. A. & EAGLESON, P. S. 1968 An asymptotic theory for water waves on beaches of mild slope. *J. Geophys. Res.* **73**, 4555–4560.

MEI, C. C. & TUCK, E. O. 1980 Forward scattering by long thin bodies. *SIAM J. Appl. Maths* **39**, 178–191.

PENNEY, W. G. & PRICE, A. T. 1952 The diffraction theory of seawaves and the sheltering afforded by a breakwater. *Phil. Trans. R. Soc. Lond.* A **244**, 236–253.

RADDER, A. C. 1979 On the parabolic equation method for water-wave propagation. *J. Fluid Mech.* **95**, 159–176.

STAMNES, J. J. 1986 *Waves in Focal Regions.* Bristol: Adam Hilger, 600 pp.

STAMNES, J. J., LØVHAUGEN, O., SPJELKAVIK, B., MEI, C. C., LO, E. & YUE, D. K. P. 1983 Nonlinear focusing of surface waves by a lens–theory and experiment. *J. Fluid Mech.* **135**, 71–94.